FREQUENCY-CONVERSION MODELING

J. M. Auerbach
C. E. Barker
D. Eimerl
K. R. Manes
D. Milam
*P. W. Milonni**
J. B. Trenholme
B. Van Wonterghem

Introduction

With respect to the rest of the Nd:glass laser system, the frequency converter is quite small in terms of weight and size. However, it is a critical component because laser fusion targets require irradiation by ultraviolet laser light to operate successfully. The frequency converter produces ultraviolet light ($\lambda = 0.351$ μm) from the infrared light ($\lambda = 1.053$ μm) generated in the neodymium-doped glass section of the laser.

As shown in Fig. 1, the basic frequency converter for tripling consists of two crystals (advanced designs have more than two crystals). The first crystal, known as the second harmonic generator (SHG), frequency doubles a predetermined amount of incident infrared (1ω) light. The frequency-doubled (2ω) light has a wavelength of 0.526 μm. The 2ω and 1ω light are then mixed in the second crystal, known as the third harmonic generator (THG) or mixer, to form ultraviolet (3ω) light at a wavelength of 0.351 μm. The output of the THG is 1ω, 2ω, and 3ω light. The proportions of light at the three wavelengths depend on the operating configuration and the intensity and phase of the input laser pulse to the converter.

The goal of frequency-conversion modeling is to produce a converter design that results in the best performance for a required output laser pulse and that is the least sensitive to operational tolerances (such as alignment) and crystal manufacturing faults (such as surface roughness).

A frequency converter requires precise tolerances. Crystals must be tilted to an accuracy of microradians, and crystal thicknesses must be accurate to millimeters to achieve desired performance. Crystal surfaces must also be finished to a smoothness of hundredths of a micron so that the energy of a 3ω laser pulse will almost completely pass through the laser entrance hole of the hohlraum.

Frequency conversion is one example of the process of three-wave mixing. The crystals used in frequency converters are anisotropic, thus, frequency-conversion modeling must take account of the directions of the principal axes of the crystals with respect to the polarizations of electric fields in three-wave mixing. Frequency conversion is optimal at a phase-matched condition. Phase matching involves placing the principal axis of each crystal of the converter at a certain angular separation from the propagation direction. This angular separation, which must be accurate to within microradians, is called the phase-matching angle. The codes used for frequency-conversion modeling calculate phase-matching angles and the variation of converter performance for departures from the phase-matched condition. In mathematical terms, phase matching means that the difference between the wave number of the output harmonic field and the wave numbers of the input harmonic fields equals zero.

We can define the phase mismatch factor Δk as follows:

$$\Delta k = 2\pi/\lambda_h - 2\pi/\lambda_f - 2\pi/\lambda_g \ , \qquad (1)$$

where λ is the wavelength in the media, h denotes the output harmonic field, and f and g denote the input harmonic fields. Here, $\lambda = \lambda_0/n$, where n is the index of refraction, and λ_0 is the wavelength in vacuum. The value of n depends on the type of crystal material, the polarization of the field, crystal orientation, the local propagation angle of the electric field, the instantaneous wavelength if it is time-varying due to phase modulation, and temperature. Modeling codes must

*Los Alamos National Laboratory, Los Alamos, New Mexico.

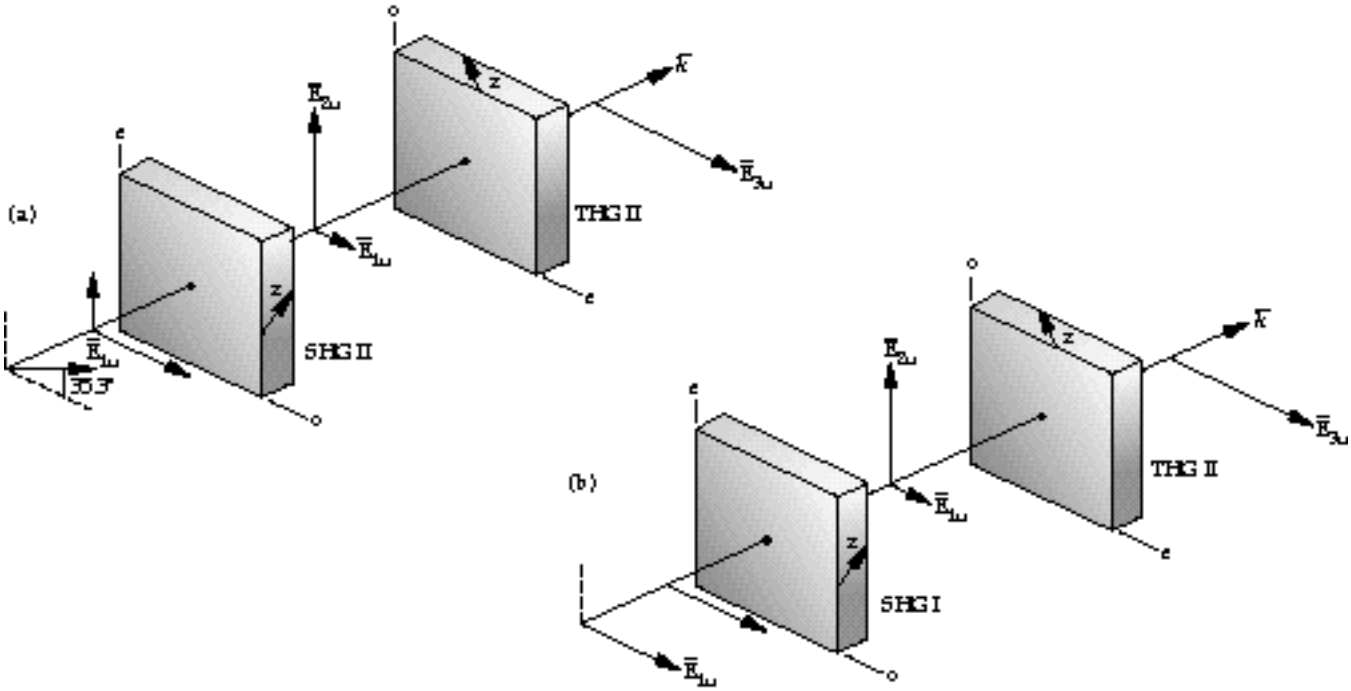

FIGURE 1. Schematic of two-crystal frequency triplers. (a) Type II/Type II crystal scheme and polarization directions for tripling. (b) Type I/Type II crystal scheme and polarization directions for tripling. 40-00-1296-2736pb01

take into account all these dependencies. Whereas $\Delta k = 0$ for phase matching, as we will show later, Δk is sometimes deliberately made nonzero in the SHG to obtain a certain amount of red and green light for the THG.

We have developed a class of frequency-conversion codes such that each code is differentiated from the others by the level of detail in the specification of the input electric field **E** to the converter. In the most general case:

$$\mathbf{E} = \mathbf{E}(x,y,z,t,\lambda_c) \ , \tag{2}$$

where, x and y are the transverse spatial coordinates, z is the coordinate in the direction of propagation, t is time, and λ_c is the center wavelength.

The different codes and electric field specifications are as follows:

1. For plane-wave steady-state fields:

$$\mathbf{E} = \mathbf{E}(z,\lambda_c) \ . \tag{3}$$

2. For plane-wave time-varying fields:

$$\mathbf{E} = \mathbf{E}(z,t,\lambda_c) \ . \tag{4}$$

3. For spatially varying steady-state fields (in three dimensions):

$$\mathbf{E} = \mathbf{E}(x,y,z,\lambda_c) \ . \tag{5}$$

4. For spatially varying and time-varying fields:

$$\mathbf{E} = \mathbf{E}(x,z,t,\lambda_c) \tag{6a}$$

for one transverse spatial dimension, and

$$\mathbf{E} = \mathbf{E}(x,y,z,t,\lambda_c) \tag{6b}$$

for two transverse spatial dimensions.

Types of Frequency Converters

The two types of crystal material used in the frequency converters for Nova, Beamlet, and the National Ignition Facility (NIF) are potassium dihydrogen phosphate (KDP) and deuterated potassium dihydrogen phosphate (KD*P). The crystals are of the negative uniaxial type.[1]

As shown in Fig. 1, each crystal can be operated in a Type I or Type II configuration. In a Type I configuration, incoming electric fields are all in one polarization direction, and the output harmonic field polarization is orthogonal to the input field's polarization. In a Type II configuration, incoming electric fields are orthogonal. The crystal axes along which the incoming electric fields are aligned are called the ordinary (o) and the extraordinary (e) axis. In the plane defined by the propagation direction and ordinary axis, there is no dependence of the index of refraction on crystal tilt angle θ. In the plane defined by the propagation direction and the extraordinary axis, the index of refraction varies with crystal tilt angle. This feature is used to adjust the phase mismatch

Δk by a process called angular detuning.

In the following discussion, we denote the electric fields involved in the three-wave mixing process by *f*, *g*, and *h*. A scalar representation can be used because each field is in one polarization, which is parallel to either the ordinary or extraordinary axis of each crystal. In a SHG crystal, *f* and *g* represent the 1ω fields, and *h* represents the 2ω field. In a THG crystal, *f* represents the 1ω field, *g* represents the 2ω field, and *h* represents the 3ω field. In a Type I SHG, *f* and *g* are parallel to the ordinary axis, and *h* is parallel to the extraordinary axis. In a Type II THG, *f* and *h* are parallel to the extraordinary axis, and *g* is parallel to the ordinary axis. From these configurations and field conventions, we can formulate equations governing the evolution of fields in the converter crystals.

Equations of Frequency Conversion

The evolution of the *f*, *g*, and *h* fields in a crystal for the most general case, with $f = f(x,y,z,t)$, $g = g(x,y,z,t)$, and $h = h(x,y,z,t)$, is determined by solving the following set of coupled, nonlinear differential equations:

$$\partial f/\partial z + 1/v_{g1}\partial f/\partial t = iC(\theta)hg^{*}e^{i\Delta kz} - 0.5\alpha_1 f + k_0[\gamma_{11}|f|^2 + 2\gamma_{12}|g|^2 + 2\gamma_{13}|h|^2]f - i/2k_f(\nabla^2 f) - \rho f\partial_f/\partial r_e \quad , \tag{7}$$

$$\partial g/\partial z + 1/v_{g2}\partial g/\partial t = iC(\theta)fh^{*}e^{i\Delta kz} - 0.5\alpha_2 g + i\lambda_1/\lambda_2 k_0[2\gamma_{21}|f|^2 + \gamma_{22}|g|^2 + 2\gamma_{23}|h|^2]g - i/2k_g(\nabla^2 g) - \rho_g\partial g/\partial r_e \quad , \tag{8}$$

and

$$\partial h/\partial z + 1/v_{g3}\partial h/\partial t = iC(\theta)fge^{-i\Delta kz} - 0.5\alpha_3 h + i\lambda_1/\lambda_3 k_0[2\gamma_{31}|f|^2 + 2\gamma_{32}|g|^2 + \gamma_{33}|h|^2]h - i/2k_h(\nabla^2 h) - \rho_h\partial h/\partial r_e \quad , \tag{9}$$

where ∇^2 is the Laplacian operator, which for Cartesian coordinates is:

$$\nabla^2 = \partial^2/\partial x^2 + \partial^2/\partial y^2 \quad . \tag{10}$$

We derived Eqs. (7–9) by starting with Maxwell's equations for a nonlinear medium. The first term on the left side of Eqs. (7–9) is the derivative in the propagation direction to be integrated. We want to calculate the evolution of the three fields as a function of *z*, the propagation direction.

The second term on the left side of Eqs. (7–9) is used only in the conversion codes that model time-varying electric fields. Here, v_{gn} is the group velocity, where $n = 1, 2, 3$. The group velocity is defined by the equation

$$v_g = \partial\omega/\partial k \quad , \tag{11}$$

where $\omega = \omega(k)$ is the dispersion relationship for a converter crystal material. The use of only v_g indicates that we are using only a first-order approximation to the dispersion relation. For the bandwidths in our modeling, this is an excellent approximation.

The first term on the right side of Eqs. (7–9) is the three-wave mixing or frequency-conversion term. (This term is included in all the types of our conversion codes.) Here, *C* is the coupling coefficient, which is a function of angle θ between the *z* axis and the principal axis of the converter crystal. The phase mismatch factor Δk is in the complex exponential. A nonzero value of Δk degrades the conversion.

The second term on the right side of Eqs. (7–9) corresponds to bulk absorption, where α_n denotes the absorption coefficients.

The third term on the right side corresponds to phase retardation arising from the nonlinear index of refraction. Note that the phase retardation for each field not only depends on its own intensity but also on the intensities of the other two fields. The quantities γ_{mn} are the nonlinear index coefficients. This term is included in all codes with temporal-field variations and/or spatial-field variations in at least one transverse dimension. It is not needed in plane-wave, steady-state codes because the uniform phase produced would have no effect.

The fourth term on the right side corresponds to paraxial diffraction. This term is included in codes where the fields vary in one or two transverse dimensions.

The fifth term on the right side is the "walk-off" factor, which is nonzero only if the field vector is in the extraordinary direction. Thus, we use the notation r_e for the coordinate in the extraordinary direction, which can be *x* or *y*, depending on the crystal configuration. The term ρ is the walk-off factor, which gives the variation of refractive index with angle θ. Walk-off accounts for the fact that, as a field propagates in a direction different from the phase-matching direction, it will no longer move with the other fields but will "walk off" from them because the index of refraction varies with direction.

Method of Solution

Equations (7–9) are solved by a split-step method to give the fields as a function of *x*, *y*, *z*, and *t* (or a subset of these variables, depending on the type of code). In this method, the derivative of each field

with respect to z is split into two components with different terms from the right hand sides of Eqs. (7–9). The integration for one component is carried out in the space–time domain, and the integration for the other component is carried out in the frequency/spatial-frequency domain. The terms in the equations are divided in the space–time domain according to:

- Frequency conversion (three-wave mixing).
- Passive loss.
- Nonlinear index phase retardation.

This part of the derivative of each field with respect to z is integrated using a fourth-order Runge–Kutta method.

The second component, which includes the time derivative of each field and the diffraction and walk-off terms, is integrated by first Fourier transforming the terms into the frequency/spatial-frequency (for x, y) domain. After the equations are transformed, they become ordinary differential equations in z instead of partial differential equations in x, y, z, t. The equations are then integrated with respect to z and inverse Fourier transformed to give the second component of the updated fields.

Thus, in Eqs. (12–14) below, we denote the angular frequency as ω and the wave numbers in the x, y , and extraordinary axes directions with κ_x, κ_y, and κ_e, respectively. After Fourier transforming the time-derivative, diffraction, and walk-off terms, the second part of the split-step solution involves integrating:

$$dF/dz = -i\omega/v_{g1}F + i(\kappa_x^2 + \kappa_y^2)/2k_f F + i\rho_f\kappa_e F \ , \qquad (12)$$

$$dG/dz = -i\omega/v_{g2}G + i(\kappa_x^2 + \kappa_y^2)/2k_2 G + i\rho_g\kappa_e G \ , \qquad (13)$$

and

$$dH/dz = -i\omega/v_{g3}H + i(\kappa_x^2 + \kappa_y^2)/2k_3 H + i\rho_h\kappa_e H \ , \qquad (14)$$

where F, G, and H denote the Fourier transforms of the second part of the split-step solution of f, g, and h. Here, κ_e can be either κ_x or κ_y depending on the orientation (x or y) of the crystal extraordinary axis. After Eqs. (12–14) are integrated with respect to z, the results are inverse Fourier transformed to give the second component of the updated fields. The two components of the fields are then added to give the total updated field after a z increment, Δz.

Outputs of the Codes

Our codes have various tabular and graphics outputs, which are illustrated below. In addition, the spatial and space–time codes can produce a file containing output harmonic and residual harmonic field distributions, which are compatible with the PROP92 propagation code. With this capability, we can propagate a converted beam through a set of optics using PROP92, as well as a 1ω beam created by PROP92 as the input 1ω field distribution for a conversion calculation.

Applications of the Frequency-Conversion Codes

Sensitivity Study of Doubler Detuning Angle by Plane-Wave Codes

As previously mentioned, the frequency-conversion crystals must be tilted with an accuracy of microradians for proper operation. This is especially true for a Type I SHG, where angular detuning is used to control the mix of 1ω and 2ω light into the THG. For design of the converter mounting and alignment equipment, it is important to know the alignment accuracy required for conversion efficiency within specifications. The variation of conversion efficiency with doubler detuning angle can be easily determined for a wide set of converter designs using the plane-wave frequency-conversion codes.

Figure 2 shows the output from a plane-wave frequency-conversion code. The plot shows 3ω conversion efficiency vs initial 1ω intensity for several values of SHG detuning angle. The latter quantity is the identifying parameter for each curve. The modeled converter configuration consisted of a 13-mm-thick KDP Type I

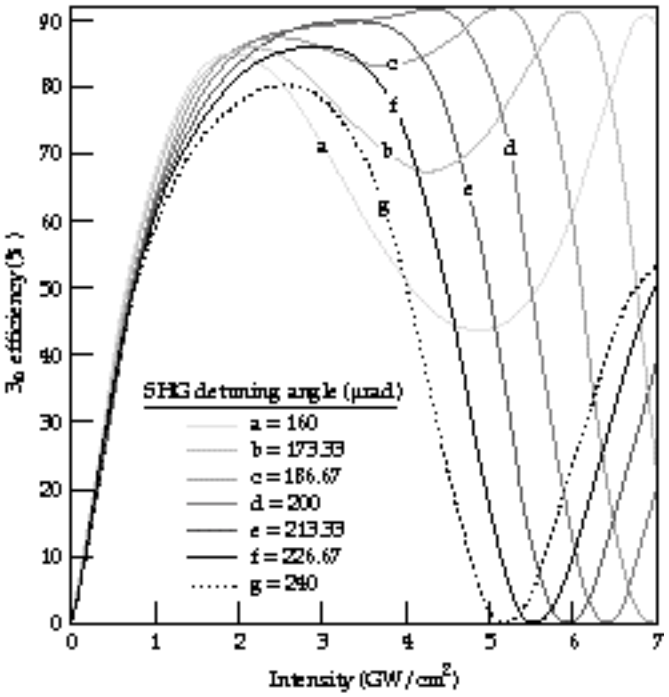

FIGURE 2. Output of plane-wave, steady, frequency-conversion code showing 3ω conversion efficiency as a function of input 1ω intensity for various doubler crystal detuning angles. 40-00-1296-2737pb01

SHG and a 11-mm-thick KD*P THG with a fixed detuning angle of 30 μrad. Notice that the sensitivity of converter performance increases with initial 1ω intensity. Thus, in considering the effect of SHG detuning angle alignment on converter performance for temporally shaped pulses, one must analyze the converter performance at the peak intensity of the shaped pulse. It is also important to note that conversion efficiency can drop off drastically as 1ω intensity increases. Decreased efficiency results from the incorrect ratio of 1ω and 2ω light into the THG. This behavior is important in the design of the dynamic range of the converter.

Effects of Applied Temporal Phase Modulation on Conversion

When phase modulation is applied to a field, $\mathbf{E}_0(z,t)$, the resulting field for a single modulation frequency f and depth of modulation σ is given by:

$$\mathbf{E}_{\mathrm{pm}}(z,t) = \mathbf{E}_0(z,t)e^{i\sigma\sin 2\pi ft} \quad . \tag{15}$$

The bandwidth bw over which the phase modulation sweeps is given by:

$$bw = 2\sigma f \quad . \tag{16}$$

As the frequency sweeps from one limit to the other, the effective wavelength of each field also changes, which affects, in turn, the phase mismatch factor [Eq. (1)]. As the phase mismatch Δk varies, the conversion efficiency varies. It is this process that turns a periodic phase modulation into an amplitude modulation.

There are two current uses for applied phase modulation on laser pulses. First, bandwidth is used to suppress Stimulated Brillouin Scattering (SBS) in large optics. The bandwidth used in this application is 30 GHz. Our conversion codes show that this bandwidth causes a small degradation in conversion efficiency, which needs to be considered along with other degrading factors.

The second application is for beam smoothing by spectral dispersion. Plans are for 1ω bandwidths in the range of 90 to 150 GHz. Our frequency-conversion codes have shown that planned converter designs suffer significant degradation in performance at such large bandwidths.

In the following examples, we show how the temporal codes model conversion of laser pulses having complex time dependencies. We show the effects of applying a 150-GHz-bandwidth phase modulation on a laser pulse having a temporal shape like that proposed for NIF indirect drive. The converter design we used consists of a 12.7-mm-thick KDP Type I SHG and a 9-mm-thick KD*P Type II THG.

Figure 3(a) shows the 3ω intensity temporal pulse shape, and Figure 3(b) shows the 1ω intensity pulse used to generate the 3ω pulse for the case with no bandwidth. The two graphs were produced by one of the temporal frequency-conversion codes. The peak 1ω intensity is 2.75 GW/cm^2. The energy conversion efficiency was calculated to be 56.5%.

The code was then run a second time starting with the 1ω pulse of Fig. 3(b); however, a phase modulation with a bandwidth of 150 GHz was impressed on the 1ω pulse. Figure 4 shows the temporal profile of intensity of the resulting 3ω pulse. The calculated energy conversion efficiency is 43.4%. Thus, the energy conversion efficiency relative to that of the pulse of Fig. 3(a) decreases by about 13%. In addition, the pulse has severe intensity modulation at twice the phase modulation frequency. The lowest intensity values correspond to times when Δk is largest in magnitude, and the peak values correspond to the times when $\Delta k = 0$. These simulations show the need for alternate converter designs for large-bandwidth operation of NIF.

One of the alternate designs is a converter with one

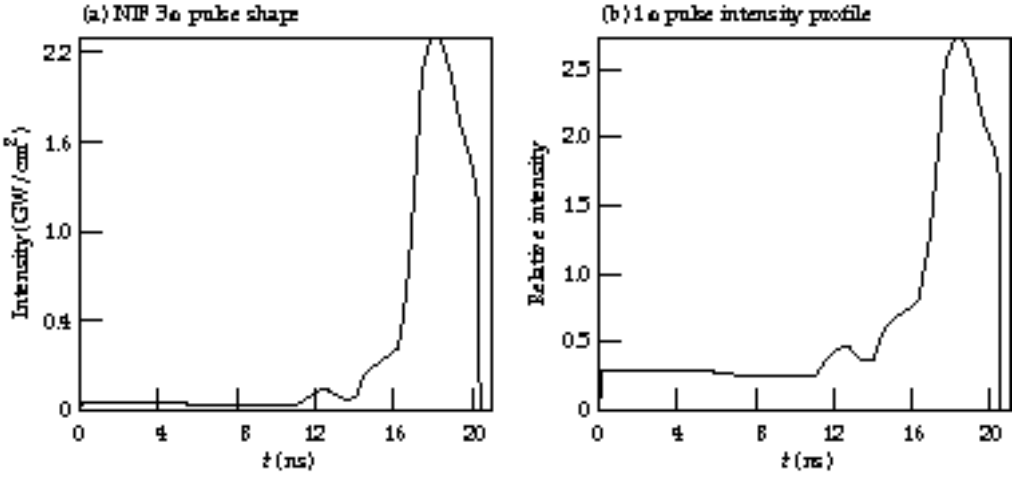

FIGURE 3. Sample output from the temporal frequency-conversion codes. (a) Temporal profile of intensity of a 3ω laser pulse with a NIF-like shape. (b) Temporal profile of intensity of the 1ω pulse derived from the pulse shape of (a) for a converter consisting of a 1.27-cm-thick KDP doubling crystal and a 0.9-cm-thick KD*P tripling crystal. 40-00-1296-2738pb01

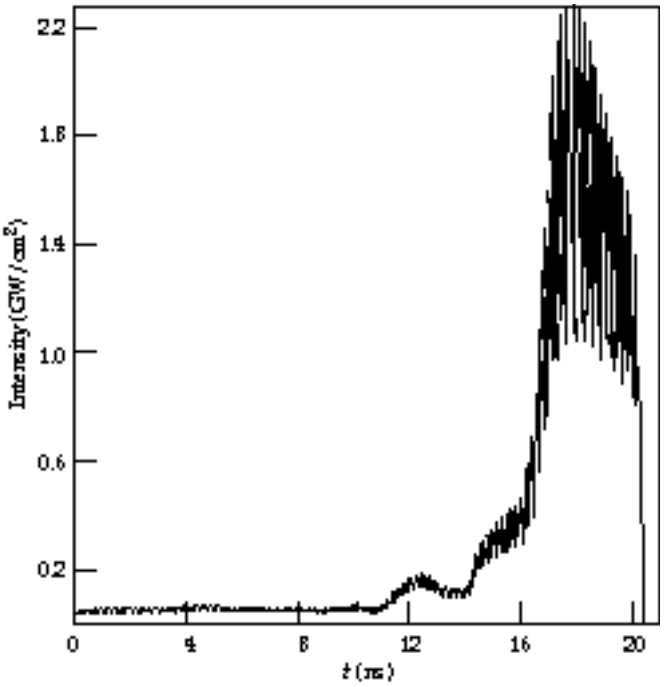

FIGURE 4. Temporal profile of intensity of the 3ω pulse produced when the 1ω pulse of Fig. 3(b) with 150 GHz of applied phase modulation is propagated through the two-crystal 1.27/0.9 converter. 40-00-1296-2740pb01

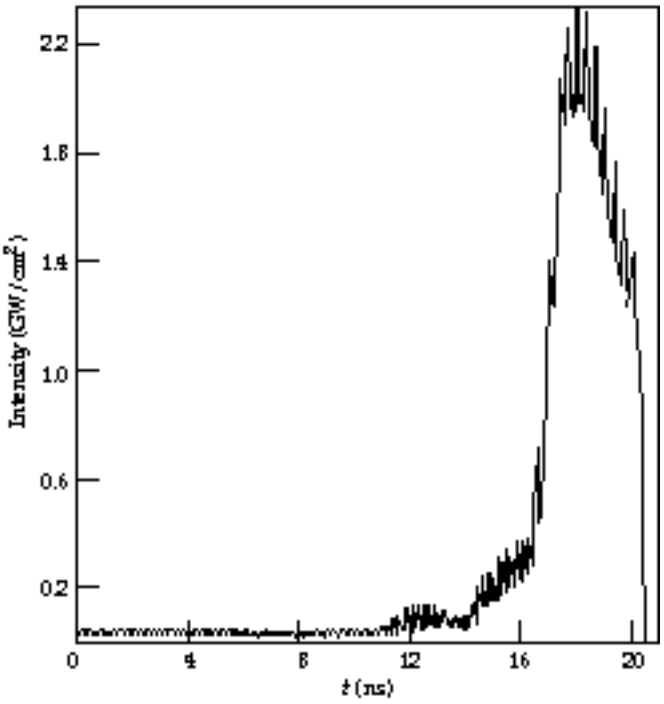

FIGURE 5. Temporal profile of intensity of the 3ω pulse produced when the 1ω pulse of Fig. 3(b) with 150 GHz of applied phase modulation is propagated through a three-crystal converter. The KDP doubler is 1.2 cm thick with a detuning angle of 210 μrad. The first KD*P tripler crystal is 0.7 cm thick with a detuning angle of 950 μrad. The second KD*P tripler crystal is 0.9 cm thick with a detuning angle of –350 μrad. 40-00-1296-2741pb01

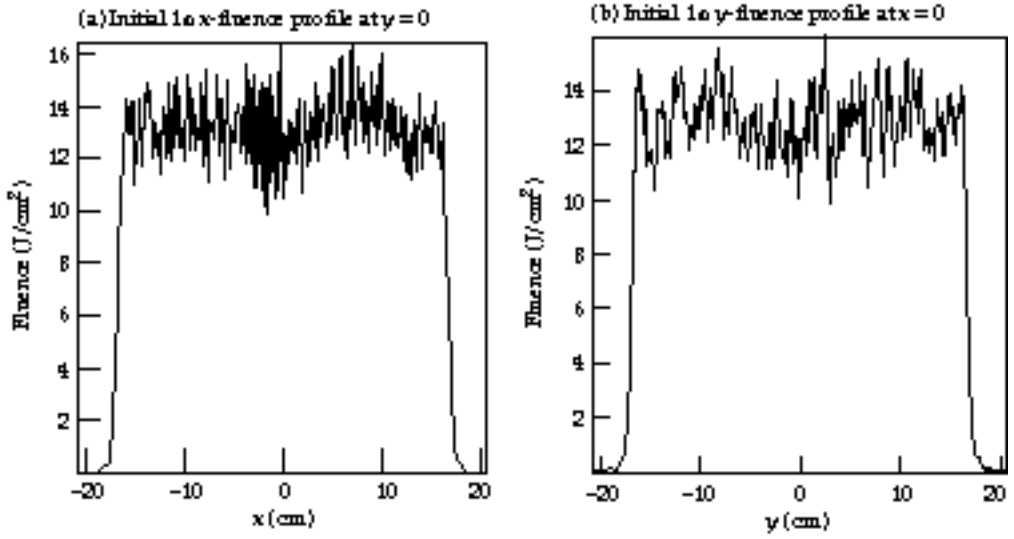

FIGURE 6. Profiles of fluence of the initial 1ω field distribution. (a) Center ($y = 0$) x profile of fluence. (b) Center ($x = 0$) y profile of fluence. 40-00-1296-2742pb01

SHG and two THG crystals. The temporal frequency-conversion code shows that this design produces a much smoother 3ω pulse, as shown in Fig. 5. In addition, the calculated conversion efficiency is 53.3%, which corresponds to a drop of only 3% relative to that of the pulse of Fig. 3(a). For higher peak intensities in the NIF-like pulse, the difference in conversion efficiency between the two-crystal design and the three-crystal design will increase.

Simulations of Field Distributions with Temporal and Transverse Spatial Variations (x, y, z, t) Using PROP92

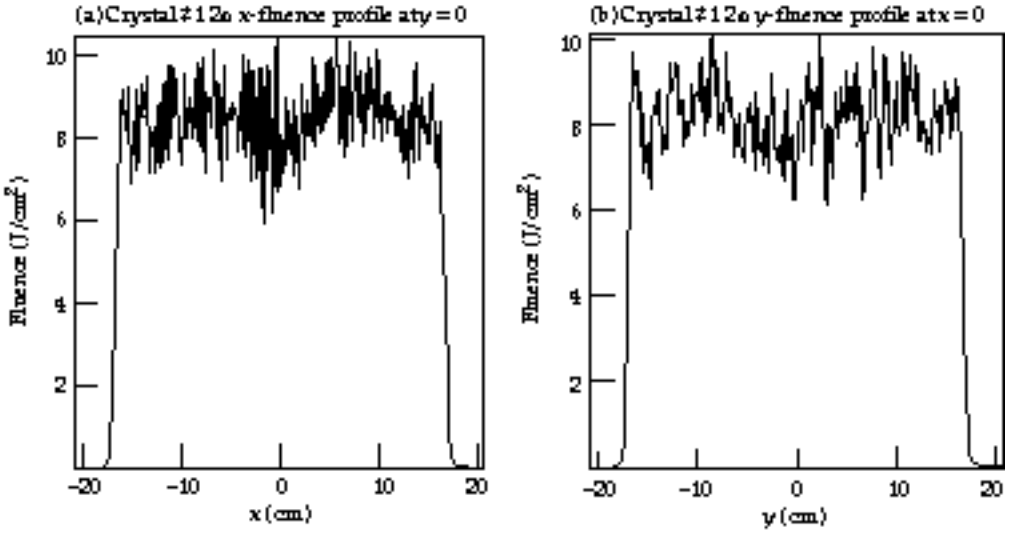

FIGURE 7. Profiles of fluence of the 2ω field distribution at the output of the doubler crystal. (a) Center ($y = 0$) x profile of fluence. (b) Center ($x = 0$) y profile of fluence. 40-00-1296-2744pb01

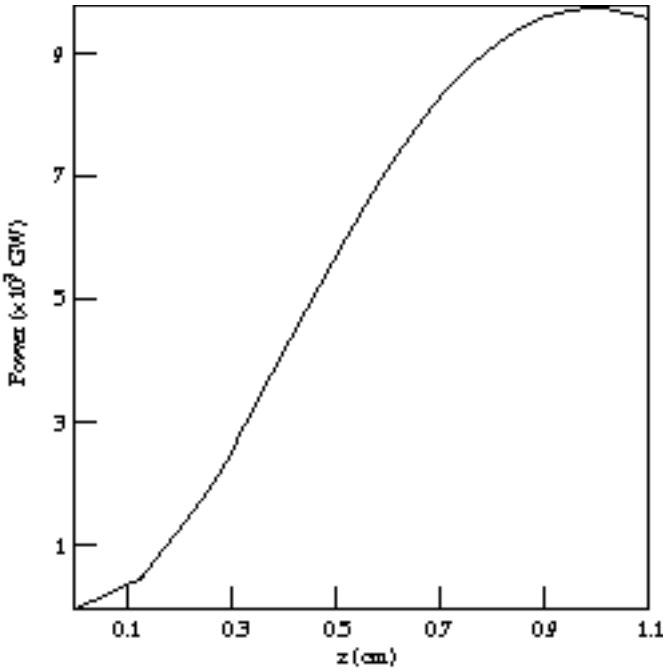

FIGURE 8. 2ω energy as a function of distance into the doubler crystal. 40-00-1296-2746pb01

The PROP92 code models the propagation of laser beams with spatial variations in one or two transverse dimensions and a temporal variation represented in a discrete set of time slices. With this temporal representation, it is difficult to model conversion of fields with applied bandwidth, but it is easy to model beams with intensity envelopes of arbitrary temporal shape and no bandwidth. However, for small bandwidths and the converter designs of interest for NIF, the effects of bandwidth are small, and results from PROP92 are quite accurate. Following is an example of the use of the frequency-conversion code for which the fields are functions of x, y, z, and Δt_n, where Δt_n denotes the time slice array.

The 1ω field distribution used in this example corresponds to simulation of a shot on the Beamlet laser system in which the 1ω output fluence is 13 J/cm^2 in a 3-ns temporally flat pulse. The pulse is represented by three time slices. The first slice corresponds to the first 0.01 ns of the pulse; the second slice to the next 2.98 ns of the pulse; and the last slice to the last 0.01 ns of the pulse. Each slice is a field distribution defined on an x–y grid. Figures 6(a) and 6(b) show the center x and y profiles, respectively, of the initial 1ω fluence. The converter used in this example consists of an 11-mm-thick KDP SHG detuned at 240 μrad and a 9-mm-thick KD*P THG. The 1ω field distributions are propagated through the SHG. Modeled physical processes include frequency conversion, nonlinear index phase retardation, paraxial diffraction, and walk-off.

Figures 7(a) and 7(b) show the center x and y profiles, respectively, of the 2ω fluence distribution. The SHG energy conversion efficiency was calculated to 63.37%. This value is determined by the internal detuning angle, which is set as close as possible to produce equal intensities of 1ω and 2ω light into the SHG. Because the fields are spatially varying, only a few grid points of the beams will meet the equal-intensity condition for a specified detuning angle. Note that the 2ω fluence modulation is almost identical in shape to the 1ω fluence modulation, indicating that intensity dominates the conversion process. This result is expected because the phase profiles from the PROP92 calculation indicate only small transverse gradients. However, with large, local transverse phase gradients (which do not apply in the present example), the walk-off term can become large and affect frequency conversion.

Figure 8 shows the 2ω energy in the doubler crystal

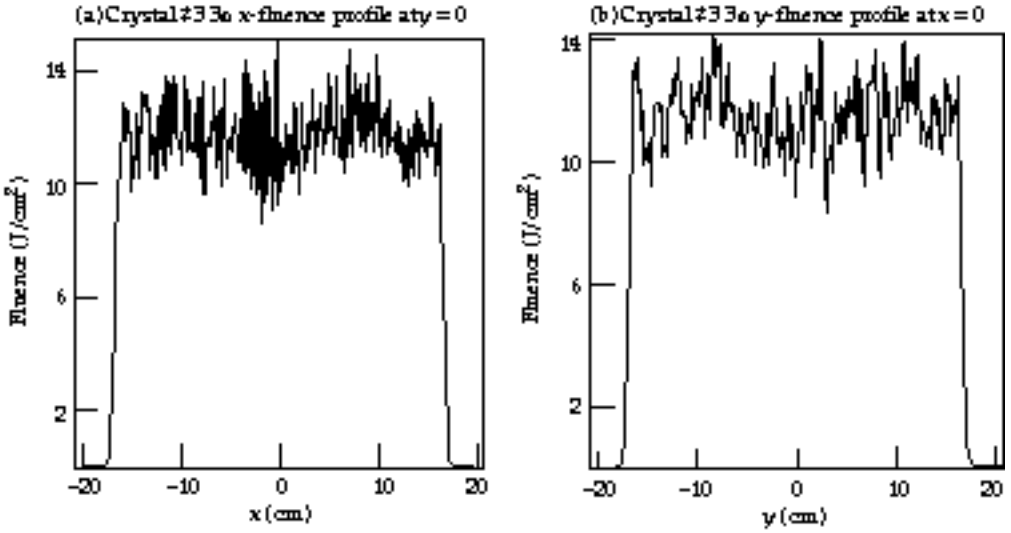

FIGURE 9. Profiles of fluence of the 3ω field distribution at the output of the tripler crystal. (a) Center ($y = 0$) x profile of fluence. (b) Center ($x = 0$) y profile of fluence. 40-00-1296-2747pb01

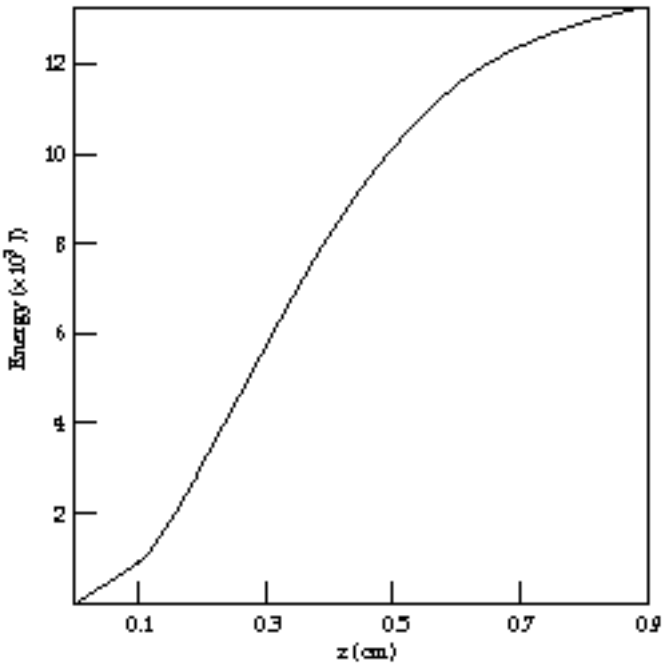

FIGURE 10. 3ω energy as a function of distance into the tripler crystal. 40-00-1296-2749pb01

as a function of distance z into the crystal. Note the slight rollover in the curve at the end of the crystal, which indicates that the detuning angle was not quite at the value for optimum conversion.

Figures 9(a) and 9(b) show the center x and y profiles, respectively, of 3ω fluence. Once again, the modulation is almost identical to that of the 1ω fluence profiles, indicating that conversion is determined mainly by the intensity distributions of the fields and not by their phase distributions. Calculated 3ω energy conversion efficiency is 88.38%. Figure 10 shows the 3ω energy as a function of distance into the tripler crystal. The 3ω field distributions calculated by this code can be used as input to PROP92 to model propagation of the 3ω beam in the output section of Beamlet and NIF. The output section extends from the output of the frequency converter to the output of the final focusing lens.

Summary

Frequency conversion is a complex nonlinear process requiring precise tolerances for optimum results. The newly developed frequency-conversion codes have aided the designers of Beamlet and NIF in specifying the correct converter designs needed for a variety of operating scenarios.

References

1. J. F. Nye, *Physical Properties of Crystals* (Oxford University Press, 1986) pp. 237–238.